Applied Ocean Research 138 (2023) 103663

Contents lists available at ScienceDirect

Applied Ocean Research

journal homepage: www.elsevier.com/locate/apor

Simplified estimation of wave attenuation in marginal ice zone using homogenized scattering model

Takahito Iida [a,*], Atle Jensen [b], Maria Zen [a]

[a] Department of Naval Architecture and Ocean Engineering, Osaka University, Suita, Osaka 5650871, Japan
[b] Department of Mathematics, University of Oslo, Oslo 0316, Norway

ARTICLE INFO

Keywords:
Water waves
Marginal ice zone
Wave attenuation
Scattering process
Dispersion relation
Homogenization
Synthetic ice experiment

ABSTRACT

A theoretical model to explain the scattering process of wave attenuation in a marginal ice zone is proposed. Although many numerical methods have been developed to accurately estimate wave attenuation, it is not easy to incorporate this knowledge and results into practical use. Therefore, a simplified estimation method is developed here to explicitly and simply describe its fundamental mechanisms. We consider a periodic array of ice floes, where the floe is modeled by a vertical rigid cylinder. Using a homogenization technique, a homogenized free surface equivalent to the array is obtained. Then, we show that a dispersion relation of the homogenized free surface waves makes all wave numbers complex. As a result, the exponential energy decay in the scattering process is demonstrated. Under the deep water assumption, the wave attenuation coefficient is proportional to the open water's wave number, ice concentration ratio, and imaginary part of the floe's heave motion. To validate the proposed theory, a tank experiment was also conducted using cylindrical synthetic ice plates. Although our model is obtained under many simplifications, the theoretical results show the same tendency and order as the experimental results.

1. Introduction

Accurate global wave hindcast is essential to utilize the ocean space. Such a wave hindcast is often based on the energy transport equation (e.g. WAVEWATCH III®; WW3DG, 2019), and a source term is represented by a linear sum of some components, such as wind–wave interaction, nonlinear wave–wave interaction, wave breaking (white-capping), and wave–ice interaction. As wave–ice interaction is likely to contribute one of the important roles to local, as well as global dynamics (Stroeve et al., 2007; Squire, 2020), an improvement of numerical and theoretical models of wave–ice interaction is demanded (e.g. Thomson et al., 2018).

Wave–ice interaction is especially of great importance in a marginal ice zone where numerous pieces of compact ice are floating on the surface of the water. Since wave energy exponentially decays with distance (Robin, 1963; Wadhams et al., 1988), wave–ice interaction is described by a wave attenuation coefficient. This attenuation is known as a result of two processes, i.e. energy dissipation and scattering (see the latest review by Squire, 2020). The dissipation covers various factors, such as viscosity, inelastic collisions, overwash, wave breaking, ice breaking, and so on, and (mechanical) energy is not conserved in this process. Viscoelastic layer models are often used to explain the dissipation process (e.g. De Carolis and Desiderio, 2002; Wang and Shen, 2010; Mosig et al., 2015; Sutherland et al., 2019). The dispersion relation of these models offers a complex wave number (Keller, 1998; De Carolis and Desiderio, 2002). This indicates that an imaginary part of the wave number yields exponential decay of wave amplitude and energy with distance. Such a dispersion relation is incorporated in global wave hindcasts to determine the wave attenuation coefficient (e.g. WW3DG, 2019). Despite their efforts, further improvement of models is still required from the view of overcoming homogeneous linear assumptions (Squire, 2020). Therefore, more investigations into nonlinear dynamics and modeling them are necessary. For example, it is reported that the collision of ice floes induces turbulence, and it results in energy dissipation (Løken et al., 2022).

The energy scattering process, on the other hand, conserves energy; propagating wave energy is just redistributed by a boundary of ice, i.e. the propagating energy decays due to wave reflection (or scattering) by ice. A single scattering model induced by a motion of a rigid ice floe was incorporated into the energy transport equation to calculate a wave attenuation coefficient (Masson and LeBlond, 1989; Perrie and Hu, 1996). Modeling of ice floe by an elastic plate (Squire et al., 1995) was introduced to the energy transport equation (Meylan et al., 1997). A multiple scattering model was developed based on an array of two-dimensional elastic plates (Kohout and Meylan, 2008; Kohout et al.,

* Corresponding author.
E-mail address: iida@naoe.eng.osaka-u.ac.jp (T. Iida).

https://doi.org/10.1016/j.apor.2023.103663
Received 10 May 2023; Received in revised form 21 June 2023; Accepted 7 July 2023
Available online 20 July 2023

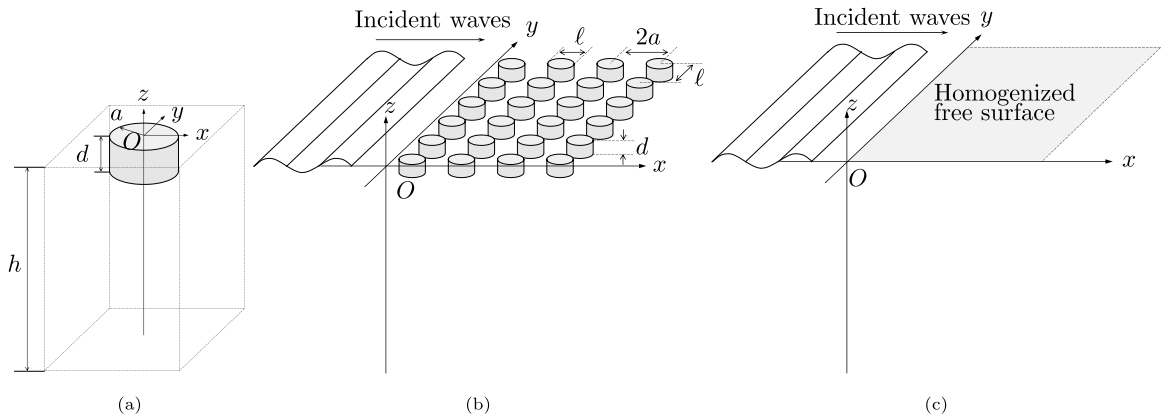

Fig. 1. Problem descriptions and concepts. (a) The local coordinate system of a single ice floe. An ice floe is modeled by a floating vertical cylinder with radius a and draft d. (b) The global coordinate system of marginal ice zone where marginal ice is modeled by a periodic array of cylinders. Distance between floes is ℓ. (c) Concept of a homogenized free surface. The periodic array of ice floes in Fig. 1(b) is replaced with the homogenized free surface. This paper aims to find such a free surface.

2011). Three-dimensional multi-body models were proposed assuming a periodic array of discs (Chou, 1998). Nonuniform distribution of floes was considered using the periodicity of a module where ice floes are contained (Bennetts and Squire, 2009; Bennetts et al., 2010). A slab-clustering method was established to calculate multiple scattering by tens of thousands of ice floes (Montiel et al., 2016). The recent developments in these numerical calculation methods have enabled us to deeply understand the scattering process of the marginal ice zone. However, it is not easy to incorporate these numerical simulations into wave hindcasts as these request high calculation costs and expertise. Therefore, a simple formula is generally preferred for application purposes. For example, WAVEWATCH III® uses fit curves of their simulations as empirical options (WW3DG, 2019).

Here, we revisit the problem of the scattering process of wave attenuation in a marginal ice zone. We propose a new scattering model that describes its fundamental mechanism in explicit and simplified manners. We believe this facilitates the fundamental understanding of the scattering process and its practical use. For a simplified estimation, we assume an ice floe is a vertical rigid cylinder, and a marginal ice zone is modeled by a periodic array of such a cylinder. Using a homogenization technique (Garnaud and Mei, 2009), a homogenized free surface equivalent to the periodic array of ice floe is obtained. This makes all wave numbers complex, and thus the wave attenuation is given in the form of an exponential function with distance. A deep water assumption results in an explicit form of the wave attenuation coefficient; the coefficient is proportional to the open water's wave number, ice concentration ratio, and imaginary part of the floe's heave motion. In addition to this, we conducted a tank experiment using a number of cylindrical synthetic ice plates. The wave attenuation coefficients are estimated in consideration of correcting the wave dissipation due to the side walls of the tank. The comparison between numerical and experimental results is shown to validate the proposed model.

2. Theoretical description

We consider a marginal ice zone consisting of discrete small ice floes with a low concentration ratio. For such a case, the process of wave attenuation is mainly described by the wave scattering (Squire et al., 1995). In the present paper, a new theoretical model is proposed to easily estimate wave attenuation due to the scattering process. The problem schematics and concepts are described in Fig. 1. A small ice floe is modeled by a truncated vertical rigid cylinder floating on the free surface as shown in Fig. 1(a). Furthermore, the marginal ice zone is modeled by a periodic array of such an ice floe as in Fig. 1(b). Here, we replace the array with a homogenized free surface equivalent to the array as in Fig. 1(c). Using this homogenized free surface, a simplified solution of the wave attenuation coefficient is proposed. The following subsections describe the details of the proposed theories.

2.1. Boundary value problem of single ice floe in waves

Firstly, a boundary value problem of a single ice floe in waves is briefly reviewed. We consider the three-dimensional coordinate system $O-xyz$ where $z=0$ plane denotes the undisturbed free surface of the water, and vertically upward is defined by positive z (see Fig. 1(a)). The sea bottom is assumed flat at $z=-h$. For simplification, the shape of the ice floe is assumed a vertical cylinder floating on the free surface, of which radius and draft are a and d. Here, only the vertical motion (heave motion) of the floe is considered. Besides, the floe is rigid, and an elastic response is not considered. We formulate the boundary value problem of the floe based on the potential flow theory (e.g. Newman, 2018); incompressible and inviscid fluid with the irrotational motion is assumed. Furthermore, plane waves with a circular frequency ω are considered. Wave amplitude and resultant floe's motion are sufficiently smaller than wavelength λ, and thus the linearization is applied. This results in the time-harmonic solutions, such as velocity potential $\Phi(\boldsymbol{x},t)=\mathrm{Re}[\phi(\boldsymbol{x})\exp(i\omega t)]$, wave elevation $A(\boldsymbol{x},t)=\mathrm{Re}[\zeta(\boldsymbol{x})\exp(i\omega t)]$, and heave motion of the floe $x_3(t)=\mathrm{Re}[X_3\exp(i\omega t)]$. Then, the linearized boundary value problem in a frequency domain is given as

$$\nabla^2\phi=0 \qquad (-h\le z\le 0), \tag{1}$$

$$\frac{\partial\phi}{\partial z}=0 \qquad (z=-h), \tag{2}$$

$$\frac{\partial\phi}{\partial z}=i\omega X_3 \qquad (z=-d), \tag{3}$$

$$\frac{\partial\phi}{\partial z}=i\omega\zeta \qquad (z=0), \tag{4a}$$

$$\zeta=-\frac{i\omega}{g}\phi \qquad (z=0), \tag{4b}$$

$$\frac{\partial\phi}{\partial z}=\frac{\omega^2}{g}\phi \qquad (z=0), \tag{4c}$$

where g is the gravitational acceleration. Here, (1) is the Laplace equation that governs the fluid domain, (2) is the sea bottom condition, and (3) is the floe bottom condition of which fluid velocity coincides with floe's velocity. Eqs. (4a) and (4b) are kinematic and dynamic conditions of the free surface, respectively. Combining (4a) and (4b), the linearized free surface condition (4c) is obtained. In addition, no flux condition is imposed for a side wall. This problem is classical, and this can be solved by any numerical simulation methods, such as an eigenfunction matching method (Miles and Gilbert, 1968; Garrett, 1971), boundary element method (Lee and Lou, 1988), and CFD. Here, the eigenfunction matching method is employed to obtain the velocity potential around the single ice floe that seeks a spectral solution using the orthogonality of eigenfunctions. The radiation, wave exciting, and

hydrostatic forces are acting on the floe due to the hydrodynamic and hydrostatic pressures (Newman, 2018). As a result, the following equation of motion is given

$$\left[-\left(1+\frac{A_{33}}{\rho\pi a^2 d}\right)+i\frac{B_{33}}{\omega\rho\pi a^2 d}+\frac{g}{\omega^2 d}\right]\frac{X_3}{\zeta_0}=\frac{g}{\omega^2 d}\frac{E_3}{\pi a^2\rho g\zeta_0}, \tag{5}$$

where ρ is fluid density, ζ_0 is incident wave amplitude, A_{33} is the added mass, B_{33} is the damping coefficient due to wave-making (not viscosity), and E_3 is the wave exciting force. Note that the equation of motion (5) is written in the non-dimensional form (using fluid density ρ, gravitational acceleration g, incident wave amplitude ζ_0, and characteristic lengths a (radius) and d (draft)) because the non-dimensional motion will be used in the later section.

2.2. Homogenized boundary value problem of waves in marginal ice zone

We assume that the marginal ice zone is modeled by an array of the floes periodically arranged in distance ℓ (see Fig. 1(b)). The floe is represented by the floating vertical cylinder as described in Section 2.1, and all floes' radii and drafts are uniforms. The radius, draft, and distance are smaller than the wavelength, or at most in the same order as the wavelength. In this subsection, we aim to model a homogenized free surface consisting of the free surface of the water and the surface of floes as in Fig. 1(c). This idea is inspired by Garnaud and Mei (2009) and Mei (2012); they developed a model for an array of point absorbers, but they implied the applicability of their model to a problem of small ice floes. Nevertheless, the point absorber has an energy extraction term which is assumed $O(1)$, and hydrodynamic forces are ignored as $O(\varepsilon)$. In the case of ice floes, on the other hand, hydrodynamic forces must be taken into account, and this influence does not appear in the leading order solution. Therefore, we shall modify the theory to bring it in line with our problem.

We focus on one floe in the array. The floe is surrounded by a unit cell of which the horizontal square area is ℓ^2. To obtain the homogenized free surface, it is assumed that the motion of the ice floe imitates a wave elevation, namely, a pseudo-wave elevation. Then, a new wave amplitude η in the local coordinate is defined as

$$\eta(r,\theta)=\begin{cases}\zeta & (r>a;\text{on water surface})\\ X_3 & (r\le a;\text{on floe surface})\end{cases}, \tag{6}$$

where (r,θ) is a horizontal coordinate from the center of the floe (local coordinate system). Firstly, boundary conditions of the pseudo-wave elevation are considered. Assuming the small draft of the floe, the floe bottom condition (3) is approximated by the Taylor-series expansion at the undisturbed free surface $z=0$ as

$$i\omega X_3=\frac{\partial\phi}{\partial z}+O(\phi d)\qquad(z=0). \tag{7}$$

We call (7) a pseudo-kinematic condition from the analogy of the kinematic condition (4a). Furthermore, we assume the floe's motion is represented by the product of non-dimensional motion amplitude and wave amplitude, i.e.

$$X_3=X_3^*\zeta, \tag{8}$$

where non-dimensional motion amplitude holds $X_3^*=X_3/\zeta_0$ which is found in (5). Note that non-dimensional motion amplitude X_3^* is calculated by (5), and this value is the same for all floes. On the other hand, the dimensional motion amplitude X_3 of each floe depends on its global position. Applying the dynamic condition for free surface waves (4b) into (8), we get

$$X_3=-\frac{i\omega}{g}X_3^*\phi\qquad(z=0), \tag{9}$$

where (9) is called a pseudo-dynamic condition. Combining (4a) and (7), a new kinematic condition is given as

$$\frac{\partial\phi}{\partial z}=i\omega\eta\qquad(z=0). \tag{10}$$

Similarly, (4b) and (9) yield a new dynamic condition as

$$\eta=-\frac{i\omega}{g}f(r)\phi\qquad(z=0), \tag{11}$$

where

$$f(r)=\begin{cases}1 & (r>a)\\ X_3^* & (r\le a)\end{cases}. \tag{12}$$

We further deform (11) by averaging wave amplitude over the surface of the unit cell. Mean wave amplitude is calculated by

$$\overline{\eta}=\frac{1}{\ell^2}\iint_{\Delta S_F}\eta ds=-\frac{i\omega}{g\ell^2}\iint_{\Delta S_F}f(r)\phi ds, \tag{13}$$

where ΔS_F denotes the surface boundary of the cell. Considering periodicity for the unit cell's surrounding boundary, velocity potential is independent of local coordinate (see Garnaud and Mei, 2009). It facilitates the calculation of (13) as

$$\begin{aligned}\overline{\eta}&\approx-\frac{i\omega}{g\ell^2}\phi\iint_{\Delta S_F}f(r)ds=-\frac{i\omega}{g}\phi\frac{1}{\ell^2}[(\ell^2-S)+X_3^*S]\\&=-\frac{i\omega}{g}[1+\psi(X_3^*-1)]\phi,\end{aligned} \tag{14}$$

where $S=\pi a^2$ is waterplane area of the floe and $\psi=S/\ell^2$ is an ice concentration ratio (a.k.a. filling ratio). Note that (14) is valid not only for a vertical cylinder but also for other geometries (such as a rectangular plate). When the cylinder is considered, the maximum concentration ratio is $\psi=\pi/4$.

Summarizing the above boundary conditions, the homogenized boundary value problem of wave propagation in the marginal ice zone is formulated as

$$\nabla^2\phi=0\qquad(-h\le z\le 0), \tag{15}$$

$$\frac{\partial\phi}{\partial z}=0\qquad(z=-h), \tag{16}$$

$$\frac{\partial\phi}{\partial z}=i\omega\zeta\qquad(z=0), \tag{17a}$$

$$\zeta=-\frac{i\omega}{g}[1+\psi(X_3^*-1)]\phi\qquad(z=0), \tag{17b}$$

$$\frac{\partial\phi}{\partial z}=\frac{\omega^2}{g}[1+\psi(X_3^*-1)]\phi\qquad(z=0), \tag{17c}$$

where wave amplitude is represented by ζ as it is a function of the global coordinate. Here, (17b) is the homogenized dynamic condition, and (17c) is the homogenized free surface condition. In the paper, we used the simplified calculation procedure. The same result is obtained using the perturbation series expansion which was used in Garnaud and Mei (2009). The difference from Garnaud and Mei (2009) is the expression of (8). As a result, only the term X_3^* in (17b) and (17c) is different from Garnaud and Mei (2009), and the others are the same.

2.3. Dispersion relation and wave attenuation in marginal ice zone

The homogenized boundary value problem (15) to (17c) is easily solved. We consider the solution for time-harmonic long-crested plane waves denoted by $A=\mathrm{Re}[\zeta\exp(i\omega t)]$ and $\zeta=\zeta(0)\exp(-i\kappa_n x)$ where $\zeta(0)$ is the wave amplitude at the measured up-wave position and κ_n is wave number of waves in the marginal ice zone. Solving the problem, we obtain the dispersion relation as

$$\frac{\omega^2}{g}[1+\psi(X_3^*-1)]=\kappa_n\tanh\kappa_n h, \tag{18}$$

where the solution of κ_n becomes complex because X_3^* is complex. When the ice floe does not exist on the surface (i.e. the concentration ratio $\psi\to 0$) or the floe is too small (i.e. $|X_3^*|\to 1$ and $\arg(X_3^*)\to 0$), (18) is deformed as

$$\frac{\omega^2}{g}=k_n\tanh k_n h, \tag{19}$$

Table 1
Wave numbers for open water k_n and for marginal ice zone κ_n at following conditions: circular frequency $\omega = 0.5$ rad/s, concentration ratio $\psi = 0.5$, non-dimensional motion amplitude $X_3^* = 9.75 \times 10^{-1} - 3.03i \times 10^{-4}$ (floe radius $a = 20$ m and draft $d = 1.0$ m), and Water depth is sufficiently deep.

n	k_n	κ_n
0	2.55×10^{-2}	$2.52 \times 10^{-2} - 3.86i \times 10^{-6}$
1	$-7.54i \times 10^{-3}$	$2.01 \times 10^{-7} - 7.56i \times 10^{-3}$
2	$-2.20i \times 10^{-2}$	$3.39 \times 10^{-7} - 2.20i \times 10^{-2}$
3	$-3.57i \times 10^{-2}$	$3.09 \times 10^{-7} - 3.58i \times 10^{-2}$
4	$-4.90i \times 10^{-2}$	$2.61 \times 10^{-7} - 4.91i \times 10^{-2}$
5	$-6.22i \times 10^{-2}$	$2.21 \times 10^{-7} - 6.22i \times 10^{-2}$

where (19) is a dispersion relation of waves on open water (ice-free) and k_n is the wave number of this relation.

The example of wave numbers is shown in Table 1. Both wave numbers for open water k_n and the marginal ice zone κ_n are calculated at the circular frequency $\omega = 0.5$ rad/s using (18) and (19). Water depth is assumed deep. The floe size is set as the radius $a = 20$ m and draft $d = 1.0$ m, and then non-dimensional hydrodynamic forces and motion amplitude are given as $A_{33}^* = 14.61$, $B_{33}^* = 5.86$, $E_3^* = 5.87 \times 10^{-1} + 1.45i \times 10^{-1}$, and $X_3^* = 9.75 \times 10^{-1} - 3.03i \times 10^{-4}$ where superscript $*$ denotes the non-dimensional values of these quantities whose non-dimensionalizations are shown in (5). Furthermore, the concentration ratio $\psi = 0.5$ is used. Table 1 shows the first six solutions. Wave number for open water has one real solution k_0 and infinite numbers of imaginary solutions $k_1, k_2, \ldots$. The wave number k_0 represents progressive waves, and $k_1, k_2, \ldots$ describe local waves whose amplitudes exponentially decay with distance, respectively. The wave number for the marginal ice zone has infinite numbers of solutions, however, all solutions are complex. This indicates that waves propagate with decaying amplitude; damped waves (e.g. Fox and Squire, 1994) are generated. Interestingly, the dominant part of κ_n (real part for κ_0 and imaginary part for others) is almost the same as that of k_n. As amplitudes of $\kappa_1, \kappa_2, \ldots$ are small and decaying rapidly, κ_0 represents the main waves in the marginal ice zone. It is also indicated that the wavelength is slightly modulated.

Now, we discuss the energy attenuation in the marginal ice zone. It is known that many field observations indicate energy decays exponentially with distance (e.g. Robin, 1963; Wadhams et al., 1988; Meylan et al., 2018). Therefore, the energy $E(x)$ may be

$$E(x) = E(0)e^{-\alpha x}, \tag{20}$$

where $E(0)$ is initial energy and α is a wave attenuation coefficient. This can be justified by considering the wave number. Here, we rewrite the wave number as $\kappa_0 = \kappa_R - i\kappa_I$ where κ_I is defined positive (for long wave frequencies). Then, wave elevation becomes

$$A(x,t) = \mathrm{Re}[\zeta(0)e^{-i\kappa_0 x}e^{i\omega t}] = \mathrm{Re}[\zeta(0)e^{-\kappa_I x}e^{i(\omega t - k_R x)}]. \tag{21}$$

Therefore, wave energy is given as

$$E(x) \propto |\zeta|^2 \propto e^{-2\kappa_I x}. \tag{22}$$

This confirms that wave energy exponentially decays with distance, and $\alpha = 2\kappa_I$.

Using deep water assumption, the result becomes simpler. The wave number in deep water is given as

$$\kappa_0 = \frac{\omega^2}{g}[1 + \psi(X_3^* - 1)]. \tag{23}$$

Therefore, the imaginary part of the wave number is explicitly obtained, and the wave attenuation coefficient becomes

$$\alpha = 2\kappa_I = -2\frac{\omega^2}{g}\psi \mathrm{Im}[X_3^*] = -2K_0\psi \mathrm{Im}[X_3^*] \tag{24}$$

where $K_0 = \omega^2/g$ is the wave number for open water in the deep sea. This indicates that the wave attenuation coefficient is proportional to wave number K_0, concentration ratio ψ, and imaginary part of the floe's motion $\mathrm{Im}[X_3^*]$. The linear relationship between the wave attenuation coefficient and the concentration ratio in the scattering process was reported in Bennetts et al. (2010). In addition, the power law relation between the wave attenuation coefficient and frequency was also proposed in Meylan et al. (2018). These results are well reproduced by this simplified model.

Using the above method, complex wave number and resultant attenuation are obtained. Similar results are given in the dissipation process through viscoelastic layer models of an ice plate (Keller, 1998; De Carolis and Desiderio, 2002). In the dissipation process, the imaginary part of the wave number is caused by viscosity; energy dissipates with the distance. On the other hand, energy is conserved in the scattering process; incident wave energy is redistributed to unsteady disturbance wave energy by the floe. Here, disturbance waves consist of scattering waves and the product of radiation waves and the floe's motion. The incident wave energy is transformed into the scattering wave energy by the existence of the floe (i.e. diffraction problem). In addition, the incident wave energy is also transformed into the energy of the motion of the floe, and this is transformed into the energy of the motion-generated outgoing waves due to the wave-making damping coefficient (i.e. radiation and motion-free problems). The total energy should be conserved, however, disturbance waves propagate radially, and the energy density fades with distance. Therefore, we ignore such disturbance waves as these waves cannot travel far, and thus it looks like energy dissipates. We emphasize that energy is just transformed into disturbance wave energy and never dissipates. As a result, (24) indicates *the attenuation of incident wave energy* along to propagation direction.

It is worth noting that incorporating the presence of objects into a dispersion relation is also studied in the field of porous structures (Yu and Chwang, 1994). They often use arrays of the bottom-mounted vertical cylinders (e.g. Molin et al., 2016; Arnaud et al., 2017), and complex wave numbers are given only when the viscous effect is considered. Furthermore, considering a porosity of an ice plate in a viscoelastic layer model, a porous viscoelastic model was proposed (Chen et al., 2019; Xu and Guyenne, 2022). These studies might be helpful to simulate the wave energy dissipation in the marginal ice zone. We emphasize that boundary layers and resultant vortex at the cylinder's side walls are not always negligible for waves through the array of cylinders (see Kagemoto et al., 2002; Antolloni et al., 2020). Nevertheless, these are not considered because our purpose is to establish the simplified estimation method of wave attenuation by the scattering process.

3. Description of experiment

3.1. Outline of tank experiment

To validate the proposed estimation method, a laboratory experiment was conducted. A two-dimensional (2D) tank at Osaka University, Japan was used for this experiment. The schematic view of the tank experiment is shown in Fig. 2(a). The tank length is 14.0 m, and the width is 0.3 m. A water level of 0.45 m was kept throughout all measurements, where fresh water was used. The plunger-type wave maker and absorber are equipped on both ends of the tank. The coordinate system $O - xz$ is defined as in Fig. 2(a) where the origin O is located at the cross-section between the wave maker on the left-hand side of the tank and the undisturbed free surface of the water. In addition, the z-axis and the x-axis are positive upward and rightward, respectively. Waves are generated by the wave maker on the left-hand side, and those waves are canceled by the wave absorber on the other side using the wave absorption control theory (Milgram, 1970) to prevent the wave reflection from the end of the tank.

We used cylindrical synthetic ice plates for this validation to investigate wave attenuation due to the scattering process. The synthetic ice plate is made of polypropylene where the density is 0.9 g/cm^3. The

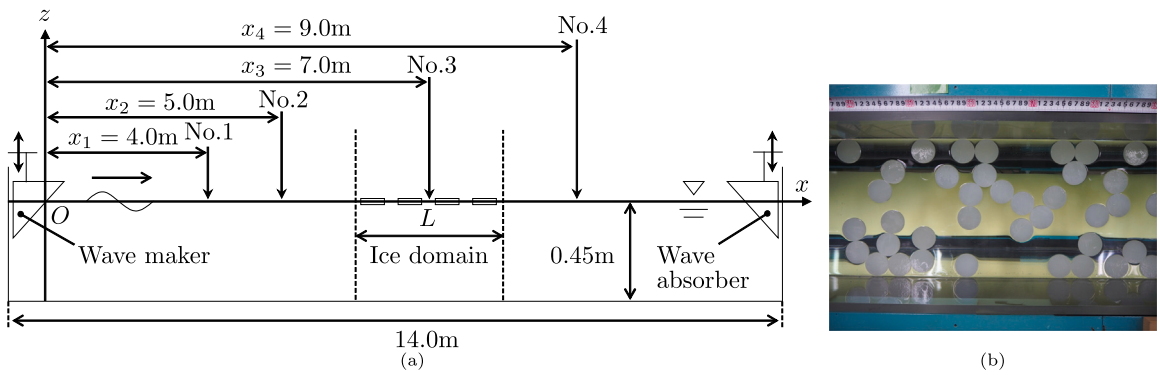

Fig. 2. (a) Schematic view of experiment in a 2D tank. Free surface elevations are measured at No. 1, No. 2, No. 3, and No. 4 (No. 3 is used only when an ice floe is not arranged). Synthetic ice plates are arranged on the ice domain where $L = 1.0$, 1.5, and 2.0 m are the ice domain length. (b) Snapshot of a top view of the ice domain. Cylindrical synthetic ice plates with a radius of 2.5 cm and a draft of 1.0 cm were randomly put on the free surface.

radius of the plate is 2.5 cm, and the thickness is 1.0 cm; the plate's draft is 0.9 cm. The numerically-calculated hydrodynamic forces and motion of this plate are shown in Appendix A. Those synthetic ice plates were arranged on the surface of the ice domain denoted in Fig. 2(a). The center of the ice domain is at $x_3 = 7.0$ m, and the ice domain length is defined by L. A snapshot of the top view of the ice domain is shown in Fig. 2(b). This experiment assumes a random arrangement of the array although the proposed model assumes a periodic array of the plates as in Fig. 1(b). Free surface elevations were measured by four ultrasonic wave probes of which the sampling frequency is 100 Hz. Those are labeled as No. 1, No. 2, No. 3, and No. 4 with corresponding distances from the wave maker $x_1 = 4.0$, $x_2 = 5.0$, $x_3 = 7.0$, and $x_4 = 9.0$ m, respectively, as in Fig. 2(a). No. 1 and No. 2 were used to measure and decompose incident waves and reflected waves from the edge of the ice domain. On the other hand, No. 4 is used to measure transmitted waves. No. 3 is only used in ice-free conditions.

In this paper, we conducted two sets of experiments. Firstly, the influence of the ice domain length L on wave attenuation was investigated. We considered three lengths $L = 1.0$, 1.5, and 2.0 m. Here, we assumed a low concentration ratio $\psi = 0.3$ to avoid wave dissipation by collision. Therefore, the numbers of ice plates are $N = 46$ for $L = 1.0$ m, $N = 69$ for $L = 1.5$ m, and $N = 92$ for $L = 2.0$ m, respectively. Secondly, the influence of the concentration ratio ψ on wave attenuation was investigated. Three concentration ratios $\psi = 0.3$, $\psi = 0.5$, and $\psi = 0.7$ were considered. Here, the ice domain length is fixed as $L = 1.5$ m. The number of the ice plates are then $N = 69$ for $\psi = 0.3$, $N = 115$ for $\psi = 0.5$, and $N = 160$ for $\psi = 0.7$. Since this experiment has uncertainty due to the random arrangement of ice plates and measurement system, we repeated the experiment 5 times for every condition.

3.2. Outline of data analysis

In this paper, we discuss the first-order quantities, especially the wave attenuation coefficient. Therefore, measured time series data are transformed into Fourier series coefficients. The analysis range of time series data is decided to avoid influences of transient wave front and wave reflection. As the target wave period is small ($T = 0.36$ to 0.8 s), the wave dissipation due to the side walls of the tank is not negligible. To remove such a dissipation, the wave dissipation ratio $C_{\mathrm{dis}}(T, |x_m - x_n|) = c_m/c_n$ $(m, n = 1, 2, 3, 4)$ is firstly measured without any synthetic ice floe (i.e. the ice-free condition), where c_m is first order wave amplitude at wave probe's position (m denotes the number of the probe). Using the dissipation ratio and the wave data of No. 1 and No. 2, amplitudes of incident waves and reflected waves from the edge of the ice domain are decomposed. We extend the decomposition method (Goda and Suzuki, 1976) to consider wave dissipation. This method is described in Appendix B. Then, the reflection coefficient C_R and transmission coefficient C_T are calculated as

$$C_R = \frac{c_R}{C_{\mathrm{dis}}(T, x_3 - x_2)C_{\mathrm{dis}}(T, x_3 - x_1)c_I},$$
$$C_T = \frac{c_3}{C_{\mathrm{dis}}(T, x_4 - x_3)C_{\mathrm{dis}}(T, x_3 - x_1)c_I}, \tag{25}$$

where c_I and c_R are decomposed incident and reflected wave amplitudes, respectively. It should be noted that those coefficients are defined at the center of the ice domain. When the ice-free condition is considered, the following energy conservation principle may be satisfied:

$$|C_R|^2 + |C_T|^2 = 1. \tag{26}$$

The wave attenuation coefficient is estimated by the transmission coefficient. Here, we assume the following relation:

$$e^{-\alpha L} = |C_T|^2. \tag{27}$$

Therefore, the wave attenuation coefficient is given as

$$\alpha = -\frac{2}{L}\log|C_T|. \tag{28}$$

4. Results and discussion

Firstly, the dissipation ratios in ice-free conditions were measured to understand the inherent dissipation characteristics of this experimental tank. The dissipation ratios at three wave probe positions (No. 2, No. 3, and No. 4) against the upwave position (No. 1) are plotted in Fig. 3(a). This indicates that the wave elevation decreases as the distance is longer, or as the wave period is shorter. Data at No. 4 show a monotonic decrease in the wave elevation as the wave period is shorter. Whereas, results at No. 2 and No. 3 have a peak at $T = 0.4$ s. In addition, the case of No. 2 exceeds 1 at $T = 0.36$ s. The experimental tank is made of acrylic plates, and the side walls warp slightly with water pressure. Moreover, the joints of the tank's plates were glued. Therefore, not only side wall friction but also these inherent features could influence wave dissipation, especially in the short wave period domain. To remove these dissipation effects, hereafter these measured dissipation ratios are used for the correction of the results (i.e. (25) is used). The corrected wave reflection coefficient C_R, transmission coefficient C_T, and total energy $|C_R|^2 + |C_T|^2$ in ice-free conditions are shown in Fig. 3(b). This indicates that the wave reflection coefficients are almost zero for all periods as there was no ice floe. In addition, the total energies are almost 1; the energy conservation principle (26) is satisfied. Therefore, the dissipation effects are well removed from the experimental results.

Secondly, the wave elevations in ice conditions were measured to estimate the wave attenuation coefficient due to ice floes. Here, the concentration ratio $\psi = 0.3$ and ice domain lengths $L = 1.0$, 1.5, and 2.0 m were considered. Corrected total energies are shown

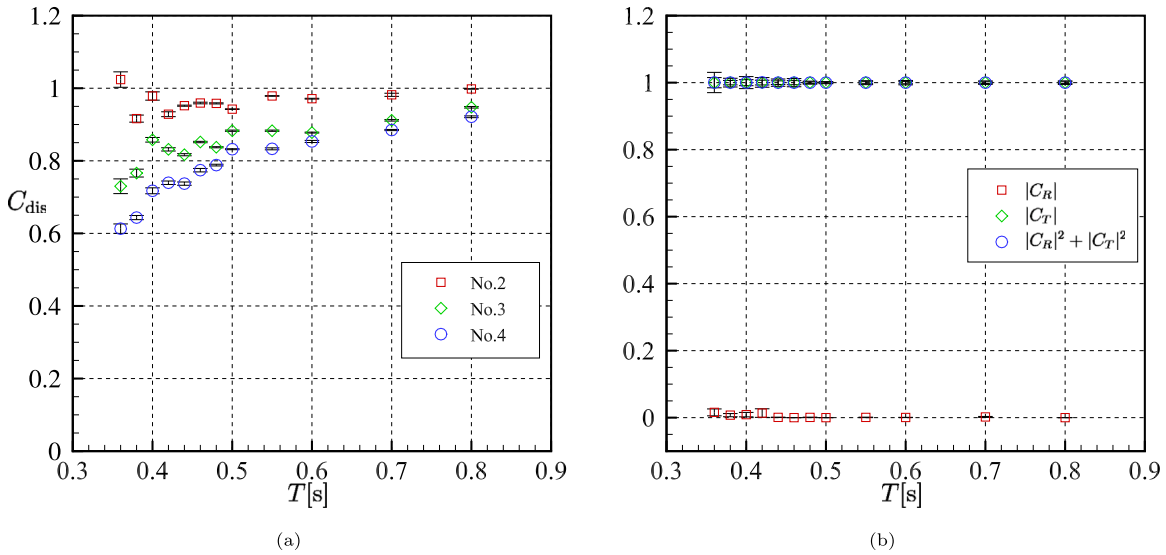

Fig. 3. (a) Experimentally measured wave dissipation ratio $C_{\mathrm{dis}}(T, x_n - x_1)$ in ice-free conditions where $n = 2, 3, 4$. Dissipation of wave elevations was measured in comparison with upwave position No. 1. (b) Reflection coefficient C_R, transmission coefficient C_T, and total energy $|C_R|^2 + |C_T|^2$ in ice-free conditions where these values were corrected by wave dissipation ratio to remove the influence of dissipation by side walls of the tank. All conditions were measured 5 times; symbols denote mean values and error bars represent standard deviations.

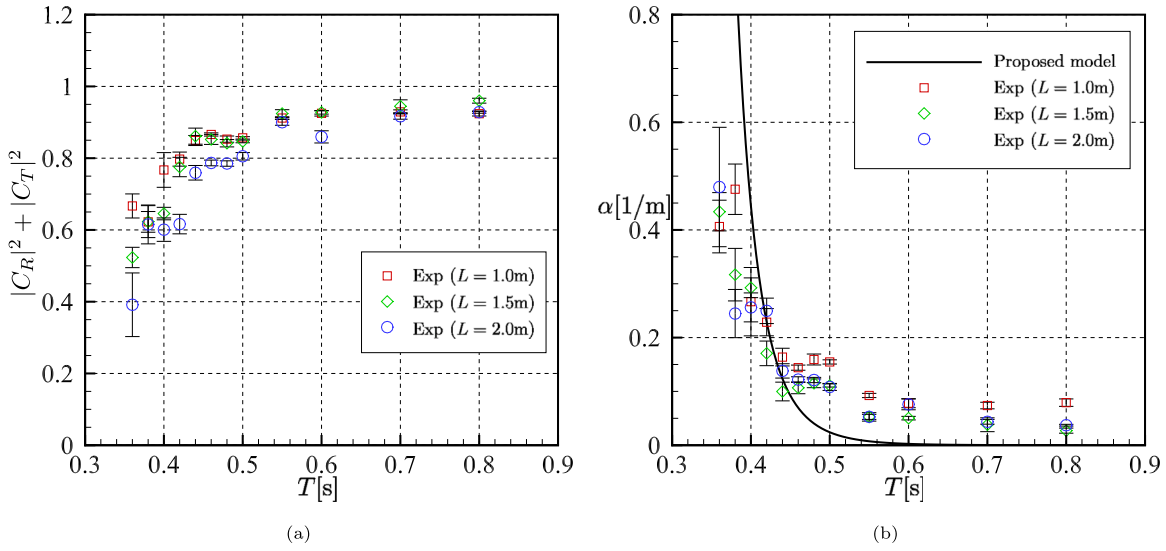

Fig. 4. (a) Experimentally measured total energy $|C_R|^2 + |C_T|^2$ in ice conditions where ice domain lengths L = 1.0, 1.5, and 2.0 m were considered. Concentration ratio $\psi = 0.3$ was considered. (b) Wave attenuation coefficients obtained by the calculation using the proposed model and experiments. All conditions were measured 5 times; symbols denote mean values and error bars represent standard deviations.

in Fig. 4(a). It should be highlighted that the total energy is less than 1 in all cases; the energy conservation principle is not satisfied. In this problem, the dissipation and scattering processes by ice floes are concerned. Viscosity and other non-conservative forces directly contribute to energy dissipation as the dissipation process. On the other hand, the wave scattering process does not ideally dissipate energy. However, such scattering waves propagate radially, and this energy density fades as distance. As a result, these waves dissipate before they reach the measuring positions, even though this is the scattering process. Note that it is difficult to decompose the cause of the experimentally measured energy dissipation into dissipation and scattering processes. Looking at Fig. 4(a), the energy dissipates more as the period is shorter. In addition, the dissipation increases as the ice domain length is longer. When the wave period is small, the deviation is large (especially, the result of $L = 2.0$ m at $T = 0.36$ s). Using the transmission coefficients, the wave attenuation coefficients are estimated. Experimental results and the numerical result calculated by the proposed homogenized scattering model are shown in Fig. 4(b). As the experimental results are calculated by (28), the wave attenuation coefficients are normalized by the ice domain length. Therefore, the results should be almost the same regardless of the ice domain length. Although the results of $L = 1.0$ m have slightly larger values than those of $L = 1.5$ and 2.0 m, almost equivalent results are obtained. The numerical result also describes a similar tendency. As for the standard deviations of experimental results, these become bigger as the wave periods are shorter. When the wave period is large ($T \geq 0.46$ s), these are small enough, and the influence of an arrangement of ice floes may be small. On the other hand, when the wave period is large (especially at $T = 0.36$ s), the standard deviation is not small, and an arrangement

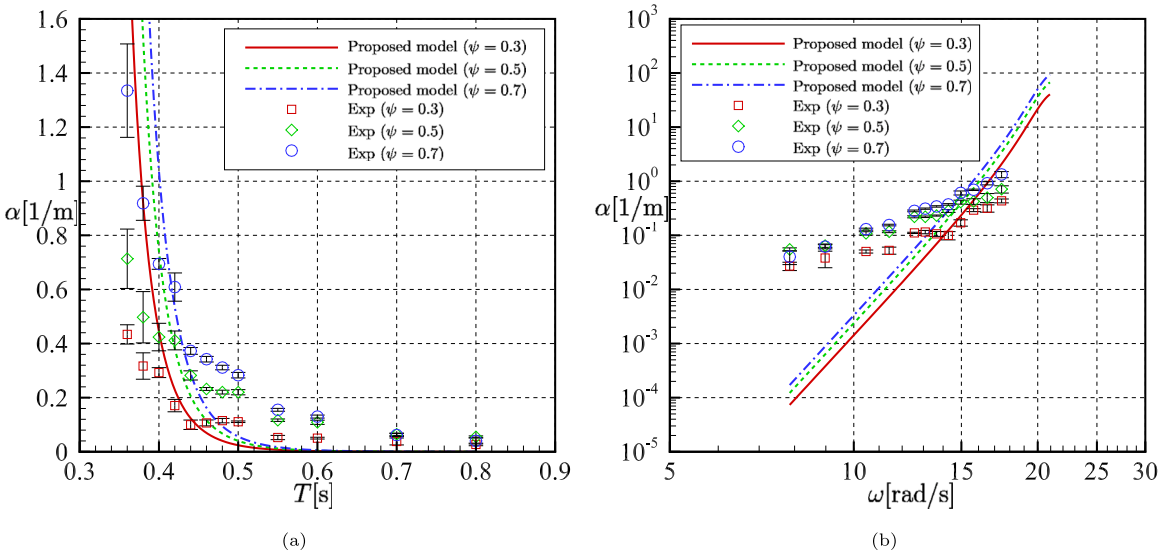

Fig. 5. Wave attenuation coefficient obtained by the calculation using the proposed model and experiments. (a) Wave attenuation coefficients against wave period in linear scale. (b) Wave attenuation coefficient against circular frequency in log–log scale. Three concentration ratios $\psi = 0.3$, 0.5, and 0.7 are compared using the ice length $L = 1.5$ m. All conditions were measured 5 times; symbols denote mean values and error bars represent standard deviations.

of ice floes could affect wave attenuation. Our theory cannot consider such a non-uniform arrangement, and only a mean value is given.

Finally, the wave attenuation coefficients were estimated by changing the concentration ratio. Here, the ice domain length $L = 1.5$ m was used, and three concentration ratios $\psi = 0.3$, 0.5, and 0.7 were considered. Those results are plotted in Figs. 5(a) and 5(b). These figures are essentially the same, but Fig. 5(a) is plotted in linear scale; Fig. 5(b) is plotted in log–log scale since the relation between the wave attenuation coefficient and circular frequency seems to obey the power law (Meylan et al., 2018). Our proposed model indicates the wave attenuation is proportional to the concentration ratio as shown in (24). The experimental results also show such a tendency. In any case, the experimental results show more attenuation than that of the numerical model at $T = 0.48 \sim 0.8$ s (i.e. $\omega = 7.9 \sim 13.1$ rad/s). Since the imaginary part of the heave motion is almost zero and the heave motion is almost 1.0 for these wave periods (see Fig. A.6(c)), incident waves are not disturbed by the ice floe. The dissipation process contributes to wave attenuation for such long waves as observed in the experiment. On the other hand, when the wave period is small, the non-dimensional wave number $k_0 a$ is not small enough, e.g. $T = 0.36$ s corresponds to $\omega = 17.5$ rad/s and $k_0 a = 0.78$. Therefore, the small floe assumption is not satisfied; the homogenized scattering model cannot estimate the wave attenuation for these wave periods. Although the applicable range is not large, the homogenized scattering model shows good agreement with the experimental results within the appropriate range.

Our proposed homogenized scattering model is based on many assumptions: only the scattering process is considered with a low concentration ratio; incompressible and inviscid fluid with the irrotational motion is assumed to consider the potential flow; wave amplitude and resultant floe motion are assumed small for linearization (wave steepness satisfies $2\zeta/\lambda \leq 1/30$); the marginal ice zone is modeled by the periodic array of the vertical rigid cylinder, and random distribution of sizes and arrangements are not considered; only heave motion of the floe is considered to assume a pseudo-wave amplitude (8); the floe's radius and draft are sufficiently smaller than the wavelength for applying the homogenization method ($k_0 a, k_0 d \ll 1$); and disturbance waves and these interactions are neglected. Therefore, we do not expect very accurate results. Instead, we expect to roughly estimate wave attenuation by the simplest model as much as possible. This is because the explicit expression would facilitate our understanding of wave attenuation in the marginal ice zone. In that sense, our model gives reasonable agreement with experimental results. In this paper, we did not discuss the influence of the water depth, and deep water is assumed throughout it. We expect that the water depth effect in the dispersion relation is almost similar to that of open water waves (see (18) and (19)).

5. Conclusion

We present a new scattering model to theoretically explain a mechanism of wave attenuation in a marginal ice zone. Our aim is not to establish a very accurate simulation model. Instead, we aim to present a theoretical model to explicitly show the fundamental characteristics of the scattering process using a simplified formulation. To make it simple, we assume the floe is a vertical cylinder, the radius of the floe is small (or at most comparable to wavelength), the draft is also small, the floe is rigid, and the floes are periodically arranged with the same distance. These assumptions as well as linear potential flow enable us to derive a homogenized free surface condition that is equivalent to the periodic array of ice floes. The resultant homogenized boundary value problem yields a new dispersion relation, and all wave numbers become complex. This indicates the exponential decay of wave amplitude and energy with distance although energy must conserve in the scattering process. Such energy inconsistency is a result of ignoring the radial waves generated by floating bodies of which amplitude decreases and vanishes with distance. Therefore, the model only shows the energy attenuation of incident plane waves. Under the deep water condition, the wave attenuation coefficient is proportional to the open water's wave number, ice concentration ratio, and imaginary part of the floe's heave motion.

In addition, a tank experiment was conducted to validate the proposed theory. Cylindrical synthetic ice plates made of polypropylene were used to uniform the condition with the theory. Because the target wave periods are too small to neglect the wave dissipation caused by the side walls of the tank, we first measured the dissipation ratios in ice-free conditions. Based on these measurements, we corrected the transmission and reflection coefficients to account for the dissipation effects. These corrected coefficients in ice conditions were measured, and the wave attenuation coefficients were estimated. The comparison indicates that the attenuation coefficients obtained by the proposed model show the same tendency and order as those by the experiments although our model is obtained by some simplifications. We believe that such a simple and explicit model may facilitate the qualitative understanding of the scattering process in the marginal ice zone.

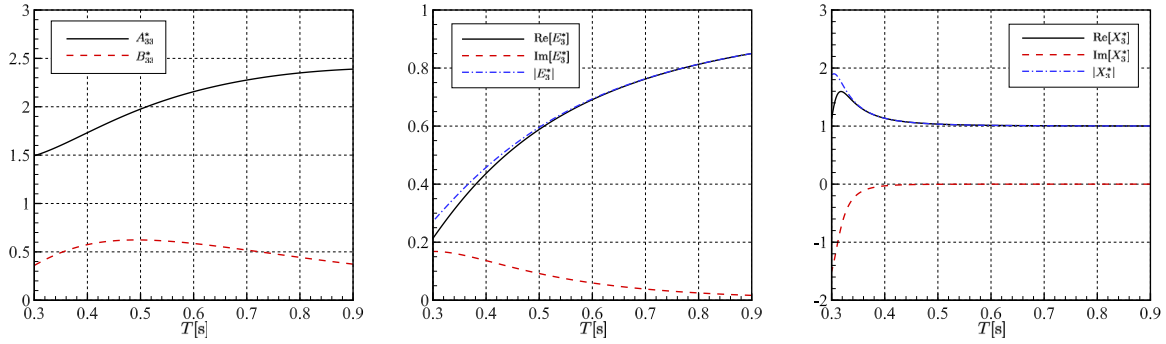

(a) (b) (c)

Fig. A.6. Wave response of a single ice plate with radius 2.5 cm and draft 0.9 cm. (a) Added mass A^*_{33} and damping coefficient B^*_{33}. (b) Wave exciting force E^*_3. (c) Heave motion X^*_3. All values on vertical axis are non-dimensionalized as in (5), while horizontal axis is dimensional wave period T s which corresponds to the experimental range. These values are calculated by the eigenfunction matching method.

CRediT authorship contribution statement

Takahito Iida: Conceptualization, Methodology, Software, Validation, Formal analysis, Resources, Data curation, Writing – original draft, Writing – review & editing, Visualization, Supervision, Project administration, Funding acquisition. **Atle Jensen:** Methodology, Resources, Writing – original draft, Writing – review & editing, Supervision. **Maria Zen:** Software, Validation, Formal analysis, Investigation, Writing – review & editing, Visualization.

Data availability

Data will be made available on request.

Acknowledgments

This work was supported by JSPS KAKENHI Grant Number JP19K15218 and 21KK0079, and Miyata Research Grant for Young Researchers. We would like to thank Prof. Junji Sawamura for providing synthetic ice.

Declaration of competing interest

The authors declare the following financial interests/personal relationships which may be considered as potential competing interests: Takahito Iida reports financial support was provided by JSPS KAKENHI Grant Number JP19K15218 and 21KK0079, and Miyata Research Grant for Young Researchers.

Appendix A. Wave response of a single ice plate

In order to calculate the wave attenuation coefficient, the non-dimensional heave motion is required. Here, this is solved by the equation of motion (5), and hydrodynamic forces are given by the eigenfunction matching method (Miles and Gilbert, 1968; Garrett, 1971). An infinite number of spectral solutions for the velocity potential are truncated up to finite numbers, and these values are decided so as to guarantee the convergence of the solution (e.g. Iida et al., 2023). In the case of an ice plate with a radius of 2.5 cm and a draft of 0.9 cm which was used in the experiment, these hydrodynamic forces and motion are given in Fig. A.6. Non-dimensional added mass A^*_{33} and damping coefficient B^*_{33} are shown in Fig. A.6(a), wave exciting force E^*_3 is in Fig. A.6(b), and heave motion X^*_3 is in Fig. A.6(c) where real part, imaginary part, and amplitude are plotted for wave exciting force and motion as these values are complex. On the other hand, the horizontal axis denotes dimensional wave period T s, and this range corresponds to that of the experiment. Note that the velocity potential and motion are exactly solved with respect to the wave period here, although the small radius and draft of the plate are assumed to obtain the homogenized scattering model.

Appendix B. Decomposition of incident waves and reflected waves

When wave reflection is expected, it is necessary to decompose incident waves and reflected waves to accurately calculate quantities. We use two time-series data measured at different positions. The first-order wave elevations at two positions are given as

$$\zeta_n = a_n \cos\omega t + b_n \sin\omega t = c_n \cos(\omega t + \theta_n) \quad (n = 1, 2), \tag{B.1}$$

where $n = 1$ is at the upwave position (No. 1 in this case), a_n and b_n are first-order Fourier series coefficients, and $c_n = \sqrt{a_n^2 + b_n^2}$ and $\theta_n = \tan^{-1}(-b_n/a_n)$ are amplitude and phase, respectively. When the wave dissipation due to side walls is considered, the incident waves ζ_I and reflected waves ζ_R are written as follows:

$$\zeta_I = C_{\rm dis}(T, x) c_I \cos(\omega t - kx + \theta_I), \tag{B.2}$$

$$\zeta_R = C_{\rm dis}(T, \ell - x) c_R \cos(\omega t + kx + \theta_R), \tag{B.3}$$

where ℓ is the distance between two wave probes, and c_I, θ_I, c_R, and θ_R are amplitudes and phases of incident waves and reflected waves, respectively. As this problem has 4 unknowns (c_I, θ_I, c_R, and θ_R) with 4 Eqs. (B.1) to (B.3), this problem can be solved. The final results are obtained as

$$c_I = \frac{1}{A}\sqrt{\frac{B^2G^2 + C^2E^2 + D^2F^2 + A^2H^2 - 2BCEG - 2BDFG + 2CDEF}{C^2 + D^2}}, \tag{B.4}$$

$$c_R = \frac{1}{B}\sqrt{\frac{A^2H^2 + C^2F^2 + D^2E^2 + B^2G^2 + 2ACFH - 2ADEH - 2CDEF}{C^2 + D^2}}, \tag{B.5}$$

where

$$\begin{cases} A = C_{\rm dis}(T, 0),\ B = C_{\rm dis}(T, \ell) \\ C = (A^2 - B^2)\cos k\ell,\ D = (A^2 + B^2)\sin k\ell \\ E = a_1,\ F = b_1 \\ G = Aa_2 - Ba_1 \cos k\ell + Bb_1 \sin k\ell \\ H = Bb_2 - Ab_1 \cos k\ell + Aa_1 \sin k\ell \end{cases}. \tag{B.6}$$

When the dissipation is not considered (i.e. $C_{\rm dis}(T, x) = 1$), the results become

$$c_I = \frac{1}{2|\sin k\ell|}\sqrt{(b_2 - b_1\cos k\ell + a_1 \sin k\ell)^2 + (a_2 - a_1\cos k\ell - b_1 \sin k\ell)^2}, \tag{B.7}$$

$$c_R = \frac{1}{2|\sin k\ell|}\sqrt{(-b_2 + b_1\cos k\ell + a_1 \sin k\ell)^2 + (-a_2 + a_1\cos k\ell - b_1 \sin k\ell)^2}, \tag{B.8}$$

and those are the same with the Goda and Suzuki (1976). Note that the results are sensitive to the experimental error of $k\ell$, and thus

$k\ell = \theta_1 - \theta_2$ is used for the analysis. It is also highlighted that the result diverges when $\sin k\ell \sim 0$. Such a case occurs if waves are not reflected (i.e. perfect transmission). Then, the results are replaced with

$$c_I = c_1, c_R = 0 \quad \text{if } |\sin k\ell| < \varepsilon, \tag{B.9}$$

where ε is a small parameter to detect divergence, and $\varepsilon = 0.2$ is used in this paper.

References

Antolloni, G., Jensen, A., Grue, J., Riise, B.H., Brocchini, M., 2020. Wave-induced vortex generation around a slender vertical cylinder. Phys. Fluids 32 (4), 042105.

Arnaud, G., Rey, V., Touboul, J., Sous, D., Molin, B., Gouaud, F., 2017. Wave propagation through dense vertical cylinder arrays: Interference process and specific surface effects on damping. Appl. Ocean Res. 65, 229–237.

Bennetts, L.G., Peter, M.A., Squire, V., Meylan, M.H., 2010. A three-dimensional model of wave attenuation in the marginal ice zone. J. Geophys. Res.: Oceans 115 (C12).

Bennetts, L., Squire, V., 2009. Wave scattering by multiple rows of circular ice floes. J. Fluid Mech. 639, 213–238.

Chen, H., Gilbert, R.P., Guyenne, P., 2019. Dispersion and attenuation in a porous viscoelastic model for gravity waves on an ice-covered ocean. Eur. J. Mech. B Fluids 78, 88–105.

Chou, T., 1998. Band structure of surface flexural–gravity waves along periodic interfaces. J. Fluid Mech. 369, 333–350.

De Carolis, G., Desiderio, D., 2002. Dispersion and attenuation of gravity waves in ice: a two-layer viscous fluid model with experimental data validation. Phys. Lett. A 305 (6), 399–412.

Fox, C., Squire, V.A., 1994. On the oblique reflexion and transmission of ocean waves at shore fast sea ice. Philos. Trans. R. Soc. Lond. Ser. A Math. Phys. Eng. Sci. 347 (1682), 185–218.

Garnaud, X., Mei, C.C., 2009. Wave-power extraction by a compact array of buoys. J. Fluid Mech. 635, 389–413.

Garrett, C., 1971. Wave forces on a circular dock. J. Fluid Mech. 46 (1), 129–139.

Goda, Y., Suzuki, Y., 1976. Estimation of incident and reflected waves in random wave experiments. Coast. Eng. Proc. 1 (15), 828–845.

Iida, T., Zareei, A., Alam, M.-R., 2023. Water wave cloaking using a floating composite plate. J. Fluid Mech. 954, A4.

Kagemoto, H., Murai, M., Saito, M., Molin, B., et al., 2002. Experimental and theoretical analysis of the wave decay along a long array of vertical cylinders. J. Fluid Mech. 456, 113–135.

Keller, J.B., 1998. Gravity waves on ice-covered water. J. Geophys. Res.: Oceans 103 (C4), 7663–7669.

Kohout, A.L., Meylan, M.H., 2008. An elastic plate model for wave attenuation and ice floe breaking in the marginal ice zone. J. Geophys. Res.: Oceans 113 (C9).

Kohout, A.L., Meylan, M.H., Plew, D.R., 2011. Wave attenuation in a marginal ice zone due to the bottom roughness of ice floes. Ann. Glaciol. 52 (57), 118–122.

Lee, C.-K., Lou, J.Y., 1988. A direct boundary-element method for three-D wave diffraction and radiation problems. Ocean Eng. 15 (5), 431–455.

Løken, T.K., Marchenko, A., Ellevold, T.J., Rabault, J., Jensen, A., 2022. Experiments on turbulence from colliding ice floes. Phys. Fluids 34 (6), 065133.

Masson, D., LeBlond, P., 1989. Spectral evolution of wind-generated surface gravity waves in a dispersed ice field. J. Fluid Mech. 202, 43–81.

Mei, C.C., 2012. Hydrodynamic principles of wave power extraction. Phil. Trans. R. Soc. A 370 (1959), 208–234.

Meylan, M.H., Bennetts, L.G., Mosig, J., Rogers, W., Doble, M., Peter, M.A., 2018. Dispersion relations, power laws, and energy loss for waves in the marginal ice zone. J. Geophys. Res.: Oceans 123 (5), 3322–3335.

Meylan, M.H., Squire, V.A., Fox, C., 1997. Toward realism in modeling ocean wave behavior in marginal ice zones. J. Geophys. Res.: Oceans 102 (C10), 22981–22991.

Miles, J., Gilbert, F., 1968. Scattering of gravity waves by a circular dock. J. Fluid Mech. 34 (4), 783–793.

Milgram, J.H., 1970. Active water-wave absorbers. J. Fluid Mech. 42 (4), 845–859.

Molin, B., Remy, F., Arnaud, G., Rey, V., Touboul, J., Sous, D., 2016. On the dispersion equation for linear waves traveling through or over dense arrays of vertical cylinders. Appl. Ocean Res. 61, 148–155.

Montiel, F., Squire, V., Bennetts, L., 2016. Attenuation and directional spreading of ocean wave spectra in the marginal ice zone. J. Fluid Mech. 790, 492–522.

Mosig, J.E., Montiel, F., Squire, V.A., 2015. Comparison of viscoelastic-type models for ocean wave attenuation in ice-covered seas. J. Geophys. Res.: Oceans 120 (9), 6072–6090.

Newman, J.N., 2018. Marine Hydrodynamics. The MIT Press.

Perrie, W., Hu, Y., 1996. Air–ice–ocean momentum exchange. Part 1: Energy transfer between waves and ice floes. J. Phys. Oceanogr. 26 (9), 1705–1720.

Robin, G.d.Q., 1963. Wave propagation through fields of pack ice. Philos. Trans. R. Soc. Lond. Ser. A Math. Phys. Sci. 255 (1057), 313–339.

Squire, V.A., 2020. Ocean wave interactions with sea ice: A reappraisal. Annu. Rev. Fluid Mech. 52, 37–60.

Squire, V.A., Dugan, J.P., Wadhams, P., Rottier, P.J., Liu, A.K., 1995. Of ocean waves and sea ice. Annu. Rev. Fluid Mech. 27 (1), 115–168.

Stroeve, J., Holland, M.M., Meier, W., Scambos, T., Serreze, M., 2007. Arctic sea ice decline: Faster than forecast. Geophys. Res. Lett. 34 (9).

Sutherland, G., Rabault, J., Christensen, K.H., Jensen, A., 2019. A two layer model for wave dissipation in sea ice. Appl. Ocean Res. 88, 111–118.

Thomson, J., Ackley, S., Girard-Ardhuin, F., Ardhuin, F., Babanin, A., Boutin, G., Brozena, J., Cheng, S., Collins, C., Doble, M., et al., 2018. Overview of the arctic sea state and boundary layer physics program. J. Geophys. Res.: Oceans 123 (12), 8674–8687.

Wadhams, P., Squire, V.A., Goodman, D.J., Cowan, A.M., Moore, S.C., 1988. The attenuation rates of ocean waves in the marginal ice zone. J. Geophys. Res.: Oceans 93 (C6), 6799–6818.

Wang, R., Shen, H.H., 2010. Gravity waves propagating into an ice-covered ocean: A viscoelastic model. J. Geophys. Res.: Oceans 115 (C6).

WW3DG, 2019. User manual and system documentation of WAVEWATCH III® version 6.07. In: Technical Note, Vol. 333. NOAA/NWS/NCEP/MMAB College Park, MD, USA, pp. 1–465.

Xu, B., Guyenne, P., 2022. Assessment of a porous viscoelastic model for wave attenuation in ice-covered seas. Appl. Ocean Res. 122, 103122.

Yu, X., Chwang, A.T., 1994. Wave motion through porous structures. J. Eng. Mech. 120 (5), 989–1008.